A measured data set for evaluating electron-beam dose algorithms

Robert A. Boyd, Kenneth R. Hogstrom, John A. Antolak, and Almon S. Shiu
Department of Radiation Physics, Box 0094, The University of Texas M. D. Anderson Cancer Center, 1515 Holcombe Boulevard, Houston, Texas 77030

(Received 8 August 2000; accepted for publication 26 March 2001)

The purpose of this work was to develop an electron-beam dose algorithm verification data set of high precision and accuracy. Phantom geometries and treatment-beam configurations used in this study were similar to those in a subset of the verification data set produced by the Electron Collaborative Working Group (ECWG). Measurement techniques and quality-control measures were utilized in developing the data set to minimize systematic errors inherent in the ECWG data set. All measurements were made in water with *p*-type diode detectors and using a Wellhöfer dosimetry system. The 9 and 20 MeV, $15\times15\,\mathrm{cm}^2$ beams from a single linear accelerator composed the treatment beams. Measurements were made in water at 100 and 110 cm source-to-surface distances. Irregular surface measurements included a ''stepped surface'' and a ''nose-shaped surface.'' Internal heterogeneity measurements were made for bone and air cavities in differing orientations. Confidence in the accuracy of the measured data set was reinforced by a comparison with Monte Carlo (MC)-calculated dose distributions. The MC-calculated dose distributions were generated using the OMEGA/BEAM code to explicitly model the accelerator and phantom geometries of the measured data set. The precision of the measured data, estimated from multiple measurements, was better than 0.5% in regions of low-dose gradients. In general, the agreement between the measured data and the MC-calculated data was within 2%. The quality of the data set was superior to that of the ECWG data set, and should allow for a more accurate evaluation of an electron beam dose algorithm. The data set will be made publicly available from the Department of Radiation Physics at The University of Texas M. D. Anderson Cancer Center. [DOI: 10.1118/1.1374245]

Key words: electron beam dose algorithm, verification data, Monte Carlo

I. INTRODUCTION

The Electron Collaborative Working Group (ECWG) developed and made publicly available an electron beam dose algorithm verification data set.[1] The purpose of the ECWG data set was to enable the evaluation of the accuracy of 3D electron pencil beam dose algorithms used for treatment planning at that time.[2,3] Recently an AAPM task group has suggested use of the ECWG data for verification of electron beam dose algorithms present in treatment planning systems.[4] Several investigators have used the ECWG data set to quantify the accuracy of more advanced electron beam dose algorithms,[5,6] while others have measured their own data set for that purpose.[7–9] At The University of Texas M.D. Anderson Cancer Center we have used the ECWG data set to evaluate modifications to the pencil-beam redefinition algorithm (PBRA).[9] Fippel *et al.* observed that the ECWG data set had inconsistent dose values at common points from different data arrays.[5] For the stepped phantom Boyd was unable to explain observed changes in off-axis depth dose in regions of side-scatter equilibrium.[10]

The purpose of the current work was to produce a more accurate measured data set, particularly for use in evaluating future modifications to the PBRA or other dose algorithms. In the current work, phantom geometries and treatment-beam configurations that simulate irregular patient surfaces, air inhomogeneities, and bone inhomogeneities were selected for measurement because our goal was to focus on evaluating the accuracy of a dose algorithm in the presence of the patient. Separate tests should be performed to test the ability of the dose algorithm to predict output (dose per monitor unit) at any point in a water phantom within the clinical range of source-to-surfaces distances (SSDs), applicator, and field size. Such a standard data set should be generated by the medical physicist at the time of commissioning an electron dose algorithm. These results may be machine dependent and should be the subject of future research.

The precision of the data was estimated by performing multiple measurements, and confidence in the accuracy of the measured data was gained by comparing the measured data with that calculated by the OMEGA/BEAM EGS4 Monte Carlo (MC) code.[11] We use the EGS4 code because of its reported accuracy and general acceptance by the scientific community. Shortt *et al.* have demonstrated the accuracy of the EGS4 code in regions distal to a localized heterogeneity.[12] However, some of the dose differences observed in the study could be attributed to use of a simple beam model (monoenergetic electrons emanating from a point source located 100 cm in vacuum from the surface of the phantom). Development of the BEAM software package has now allowed researchers to realistically model clinical electron beams with the EGS4 code. Initial studies by Rogers *et al.* have shown how BEAM can model the geometries of an accelerator head and produce complex phase spaces that result in improved

TABLE I. Description of the 14 measurement configurations.

Configuration	Phantom geometry	SSD (cm)	Energies (MeV)
1	Water	100	9
2	Water	110	9
3	Water	100	20
4	Water	110	20
5	Horizontal air slab	100	9
6	Horizontal air slab	100	20
7	Vertical air slab	100	20
8	Horizontal bone slab	100	9
9	Horizontal bone slab	100	20
10	Vertical bone slab	100	20
11	2 cm stepped surface	102	9
12	2 cm stepped surface	102	20
13	Nose-shaped surface	102	9
14	Nose-shaped surface	102	20

dose calculation accuracy in water.[11] Kapur *et al.* have shown the accuracy of BEAM in predicting clinical electron beam dosimetry, particularly output factors for a wide range of energies, applicators, and field inserts,[13] and Bieda has studied the efficacy of the BEAM code for commissioning clinical electron beams in accordance with AAPM Task Group 25.[14,15]

The measured data in the present work is assumed the ''gold standard'' and will be used to study the effect of modifications to the PBRA on dose accuracy. However, our ultimate goal is to understand the accuracy of the PBRA for patient dose calculations. MC has the ability to calculate dose in complex media, such as one presented by a patient, where measurement of the dose distribution is not possible. In this study we are able to compare measured and MC generated two-dimensional dose distributions in regions distal to localized heterogeneities and surface irregularities, thereby giving us confidence in our MC technique and allowing us to use it to generate patient dose distributions in the future. Because of the utility of this measured data set in electron dose algorithm development, it will be made available publicly for other's use through our institution.

II. MATERIALS AND METHODS

A. Measured data set

The measured data set consisted of geometric configurations similar to those of the ECWG data set. Measurements were taken in a water phantom for nominal SSDs of 100 and 110 cm. The data set also included measurements in a water phantom containing internal inhomogeneities that simulated air and bone and with irregular surfaces (stepped and nose shaped). Low-energy (9 MeV) and high-energy (20 MeV) electron beams were utilized to permit evaluation of any energy-dependent deficiency in an electron beam dose algorithm. Table I lists the 14 unique configurations in the measured data set.

Measurements were performed using a single Varian Clinac 2100C (Varian Oncology Systems, Palo Alto, CA) having a Series III electron foil/applicator set. Unlike the ECWG data set that utilized machines at two separate facilities, use of a single machine eliminated any errors in consistency that might otherwise have occurred from using different machines (e.g., differences in electron-beam energy). All measurements were made with a $15\times15\,\mathrm{cm}^2$ open applicator, which provided uniform irradiation in the regions containing the irregular surfaces or inhomogeneities. All measurements consisted of a dose distribution in a plane in the water phantom that contained central axis and was perpendicular to the edges of the applicator (collimator angle$=0°$).

TABLE II. Physical properties of materials used in phantom geometries.

Material	Density	Elemental composition
Styrofoam	$0.0265\ \mathrm{g\,cm^{-3}}$	H-0.18%, C-2.20%, N-73.70%, O-22.65%, Ar-1.27%
SR4 hard bone	$1.66\ \mathrm{g\,cm^{-3}}$	H-4.45%, C-29.09%, N-3.88%, O-31.93%, Na-0.06%, Mg-0.21%, P-10.0%, S-0.32%, Cl-0.06%, Ca-19.99%

1. Internal inhomogeneity experiments

Two slabs, one consisting of SR4 bone substitute[16] ($\rho=1.66$) to model hard bone and one consisting of Styrofoam ($\rho=0.0265$) to simulate air, were used for the internal inhomogeneity experiments. Table II provides the elemental composition of Styrofoam and SR4 bone. The dimensions of each slab were $1\,\mathrm{cm}\times3\,\mathrm{cm}\times18\,\mathrm{cm}$; the long axis was placed perpendicular to the measurement plane. An acrylic clamping device, attachable to the walls of the water phantom, was used to hold each slab in place by clamping at the ends of its long axis inside the water phantom. The clamping device, located completely outside the irradiated volume, allowed us to localize the slab at the desired depth. The slab was positioned such that its proximal end was 1 cm from the water surface. As shown in Figs. 1(a) and 1(b), each slab was oriented with its 3 cm width placed both perpendicular (horizontal) and parallel (vertical) to the beam axis, respectively. Only the 20 MeV beam was used for experiments involving the vertically oriented slabs. The SSD to the water surface was 100 cm for each of these experiments.

2. Surface irregularity experiments

Styrofoam blocks were used for experiments involving irregular surfaces. The Styrofoam blocks were abutted to the distal end of the electron applicator and partially submerged in the water phantom; this positioning displaced water into the desired surface shape. Figure 1(c) shows the configuration of the nose-shaped-surface experiment, and Fig. 1(d) shows the configuration of the 2 cm stepped-surface experiment. The SSD in each experiment was 102 cm. The Styrofoam block used for the nose-shaped-surface experiment had a pit drilled into the center such that the displaced water formed a prism (2 cm base, 3 cm height, 4 cm length) identical to the dimensions of the acrylic prism used in experi-

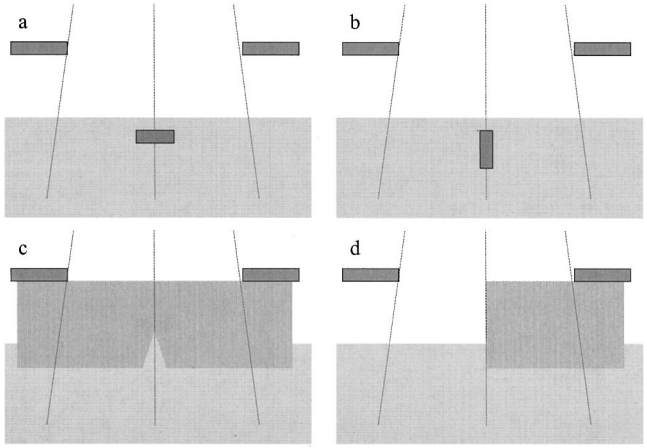

FIG. 1. Schematic of the internal slab inhomogeneities for the horizontal experiments (a) and vertical experiments (b), of the nose-shaped-surface experiment (c), and the 2 cm stepped-surface experiment (d). The edge of the electron-beam field is shown with a dotted line. The Styrofoam blocks were abutting the applicator and partially immersed in water to create the desired surface.

ment No. 9 of the ECWG data set. Trapped air bubbles were removed from the Styrofoam–water interface before measurements were performed.

B. Dose measurement methods

A *p*-type diode detector was used in conjunction with a commercial dosimetry system to collect the dose distributions. Rigorous quality control was practiced during the taking of measurements to ensure a high level of accuracy and precision in the data set. In each experiment, off-axis dose profiles were scanned at incremental depths in a transverse plane containing the central axis. A central-axis or off-axis depth dose was also scanned in each experiment. Data processing consisted of smoothing off-axis dose profiles and depth-dose curves from which two-dimensional (2D) dose distributions were constructed.

Dose was measured in a water phantom using two *p*-type silicon diode detectors (Scanditronix Medical AB, Uppsala, Sweden) in conjunction with a Wellhöfer dosimetry system (Wellhöfer Dosimetrie, Schwarzenbruk, Germany). The Wellhöfer system allows for continuous scanning with one stationary detector used as a reference detector and one scanned detector used for point measurements (0.3 mm data point spacing). The effective detection diameter of the diode detector is 2.5 mm, which allows for high spatial resolution in relative electron dosimetry. The thickness of the detector's sensitive volume is approximately 60 μm. The effective depth of the field detector was approximately 0.6 mm below the front surface of its outer shield. This was determined by comparing the diode-measured depth dose with the depth dose measured using a 0.1 cm^3 cylindrical ionization chamber (PTW, Freiburg, Germany). In both cases, dose and detector position were determined according to AAPM Task Group No. 25 protocol.[15]

Rigorous quality control was practiced during the taking of measurements to ensure a high level of accuracy and precision in the data set. Before each measurement session, the diode was positioned to match the depth of the 50% dose (R_{50}) on the central axis in water for the energy used. Lateral scans were performed to ensure that the origin ($x=0$) of the measured profile was centered between the 50% relative dose values in the penumbra and that the off-axis dose values were symmetric about the central axis. The effect of evaporation of water from the tank was minimized by adding water every hour to match R_{50}, which had been determined at the beginning of the measurement session.

The inhomogeneity slabs were positioned 1 cm from the water surface using a mechanical distance indicator attachable to the collimator. The slab position relative to the field diode was verified using a pointer attachable to the diode. The positioning reproducibility of the slabs was approximately 0.3 mm relative to the field diode. Lateral scans were then utilized to center the inhomogeneity slabs along the beam central axis. The nose-shaped surface block was also centered on the central axis using profile scans, and the stepped-surface block was positioned using the cross hairs of the light field. Offsets remaining in the measured profile scans were further corrected during postprocessing by symmetrization described below.

Dose perturbations due to irregular surfaces and internal inhomogeneity slabs were negligible at 5.0 cm lateral to the central axis. Therefore, a depth-dose curve, which was scanned 5.0 cm lateral to the central axis after the phantom geometry was set up, was used to normalize the off-axis dose profiles. The normalization minimized the effects of temperature on the signal of the diode. Off-axis dose profiles were scanned in the measurement plane, starting 5 mm below the water surface or slab and proceeding at 5 mm increments without and 2.5 mm increments with inhomogeneities present to a depth where the maximum dose was less than 5% (relative to the maximum depth dose in homogeneous water). The off-axis profile scan rate, which could be adjusted interactively, ranged from 1.23 $mm\,s^{-1}$ in regions of sharp lateral-dose gradients to 3.75 $mm\,s^{-1}$ in regions of low-dose gradients to minimize scan times and noise. Fluctuations to the water level due to the mechanical motion of the detector and mount were unobserved during profile scans. The machine ''dose rate'' during the off-axis profile and depth-dose scanning was 4 $Gy\,min^{-1}$.

As explained in Sec. II E, measured data were normalized to the maximum dose on central axis in a water phantom (without inhomogeneity) at 100 cm SSD. This was accomplished by measuring the depth dose at $x=5$ cm in the inhomogeneous phantom and normalizing it to the maximum central axis depth dose reading in water. These two depth doses were measured sequentially so that changes in ambient conditions would not affect the data. Off-axis readings were normalized to the reading at $x=5$ cm. Again, each off-axis scan took little time making this data insensitive to changes in ambient conditions. As explained in Sec. II C, the 2D dose distributions were constructed from the product of the off-axis ratios and the depth dose at $x=5$ cm.

C. Measured data processing

During postprocessing, the measured dose profiles were smoothed and symmetrized to reduce noise. The data were initially smoothed using a sliding window second-order polynomial fit available in the Wellhöfer software. The width of the window encompassed 15 data points (4.5 mm total grid width). Except for the stepped-surface data, all off-axis profile scans were symmetrized about the central axis. The off-axis profile scans were converted to ASCII text format to allow further modification by an in-house FORTRAN program. The program shifted the data such that the edges of the dose perturbations due to the inhomogeneity in the central ± 5 cm of the beam were symmetric. Afterwards, doses were interpolated to a 1 mm grid spacing, and doses at equal distances from the central axis were averaged. The same procedure was used for data outside the central ± 5 cm, using the 50% off-axis ratio for symmetrization. The centering did not require shifts greater than 0.4 mm but was necessary to fully symmetrize the data without degrading the dose perturbations and penumbra. A 2D dose distribution for each experiment was generated from the collection of processed off-axis profile scans. The grid spacing of the processed 2D dose distribution was 1 mm in the direction perpendicular to the beam axis. The consistency in the data set was assured by normalizing all profile scans of similar beam energies and SSDs with a single off-axis (5 cm) depth-dose scan.

Each experiment was repeated on two different days to further smooth noise in the data and to estimate the precision of the processed data. The three data sets of each experiment were used to calculate a mean dose and standard deviation of the mean dose at each grid point of the postprocessed dose grid matrix.

D. Monte Carlo dose calculations

Confidence in the accuracy of the measured data set and its freedom from systematic errors were gained by comparing the measured data set with MC-calculated dose distributions. The MC software package BEAM was used to model the Clinac 2100C accelerator and to collect a phase space at the distal end of the applicator. The BEAM program DOSXYZ was then used to calculate the dose distributions in the same plane as the measured data.

The geometry of the detector and the scan grid must be considered when defining the dimensions of the dose-calculation grid. The pixel width in the lateral direction was 2.5 mm to best match the effective diameter of the diode detector and to be able to model exactly the lateral dimension of the heterogeneous media with voxels of uniform density. The depth spacing was 1 mm for the 9 MeV beam and 2 mm for the 20 MeV beam. To achieve better statistics, the slice thickness of the calculation plane was 1 cm except for the nose-shaped-surface experiment. The slice thickness of the calculation plane in the nose-shaped-surface experiment was 0.5 cm due to the 4 cm length of the nose shape perpendicular to the calculation plane.

The BEAM calculations utilized many of the results of Bieda,[14] who modeled a Varian Clinac 2100C with design and dose specifications identical to those used in this study. The physical characteristics of the accelerator head were modeled with component modules of the BEAM system using information supplied by Varian Oncology Systems under a nondisclosure agreement. An additional BEAM module was used to accurately model the sharp geometry of the nose. An electron source with a Gaussian spatial distribution (1.5 mm full-width at half maximum) was utilized in the BEAM accelerator model.[14,17] The incident energy at the exit window of the accelerator was assumed to be monoenergetic and was determined by manually adjusting the energy until the calculated and measured central-axis depth of R_{50} in water matched to within 0.2 mm.

The EGS4-run parameters were set for both collection of the phase space and subsequent dose calculation as follows: AE=ECUT=0.70 MeV, AP=PCUT=0.010 MeV, and ESTEP=0.04. Approximately 5×10^8 histories were simulated from the electron source to achieve a less than 1% standard deviation in the mean dose for each experimental configuration. The maximum calculated dose $D_{\max}$ per incident electron on the central axis in water at 100 cm SSD was used to normalize subsequent MC dose calculations for heterogeneous phantoms. Data in the $D_{\max}$ region of the MC-generated central-axis depth doses in water (open field, 100 cm SSD) were fitted to a curve to determine the maximum dose per incident electron on the central axis. The precision (one standard error) of the normalization dose was estimated to be 0.2% for the 20 MeV data and 0.1% for the 9 MeV data. The MC data were symmetrized about the central axis in all but the stepped-surface experiments.

E. Data normalization and reporting of standard error

All measured and calculated data were normalized such that 100% equalled the maximum central-axis dose for an open $15\times15\,\mathrm{cm}^2$ electron field incident on a water phantom at 100 cm SSD. This resulted in a relative dose value per monitor reading for the measured data and a relative dose per incident electron for the calculated data. For the measured data the reported uncertainty is the standard error of the mean of the multiple measurement sessions. For the MC calculations, the reported uncertainty is the standard error output by the program adjusted by the normalization value. For example, a value of $25\%\pm1\%$ indicates the mean dose was 25% of the maximum central-axis dose in water and that the standard error was 1% of maximum central-axis dose in water, i.e., 4% of the 25% dose value at that point.

F. Comparison of measured dose with MC-calculated dose

The measured data were evaluated by comparing the measured dose to the MC-calculated dose on a point by point basis. The MC-calculated dose is the dose averaged over a dose grid voxel; for this comparison, it is assumed that the dose gradient across the voxel is such that the volume-averaged dose equals the dose at a point in the center of the voxel. The MC dose grid resolution was 2.5 mm laterally and 1 mm in depth at 9 MeV and was 2.5 mm laterally and

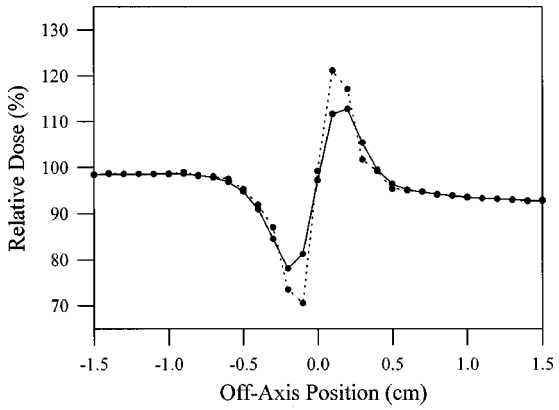

FIG. 2. 20 MeV, 2 cm stepped-surface experiment. Profile comparison in the central region at the 0.5 cm depth: raw data (solid line) and deconvolved data (dotted line).

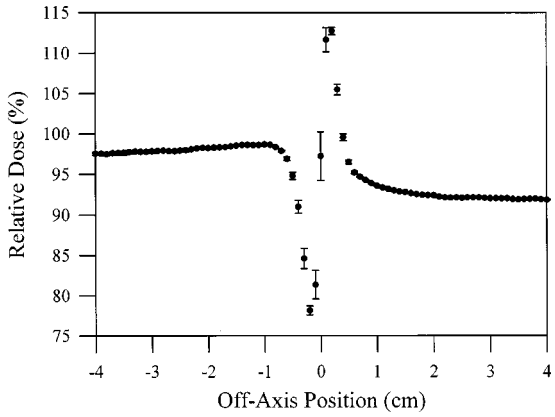

FIG. 3. Dose profile at the 0.5 cm depth for the 20 MeV stepped-surface experiment. Error bars indicate one standard deviation of the mean measured dose at each point.

2 mm in depth at 20 MeV. The measured-dose grid resolution was 1 mm laterally and 2.5 mm in depth. Bilinear interpolation of the measured data were used to determine the measured dose at the center of each MC dose voxel for calculating dose differences. The distance to agreement (DTA) was also calculated for each dose point on the MC dose grid.

Measured and calculated 2D dose distributions were compared visually, allowing one to qualitatively evaluate the similarities between the data, by overlaying plots of isodose contours at 10% intervals, starting at the 10% contour. Throughout the results, the calculated isodose contours are represented by solid curves, and the measured isodose contours are represented by dashed curves.

G. Impact of detector size

The diode used for field measurements has an actual diameter of 2.5 mm, which according to García-Vincente *et al.*[18] has a line-spread function that can be modeled by a Gaussian distribution with a full-width at half maximum equal to 2.25 mm. The 20 MeV stepped-surface data is useful for examining the effects of the spatial response of the diode detector. By deconvolving the data, the point dose is better estimated. Figure 2 shows the profile comparison between the raw and deconvolved data at the 0.5 cm depth. The dose differences in the minimum and maximum dose peaks were 10%. The data were not deconvolved in the present work. This is appropriate for the Monte Carlo comparisons, because those calculations had a bin resolution in the direction of the dose gradients of 2.5 mm.

III. RESULTS AND DISCUSSION

A. Precision

The measured depth-dose data in water (without inhomogeneity) showed a high level of precision. The average standard error of the mean measured dose was typically 0.2% for the 20 MeV data and 0.3% for the 9 MeV data in regions of low dose gradients. Deviations greater than 1% did occur at a few points in regions of high-dose gradients; extreme cases are illustrated below. Figure 3 shows the precision of the 20 MeV stepped-surface data at the 0.5 cm depth. On the central axis, the standard error of the mean dose was 3%. Figure 4 shows the precision of the 9 MeV air-slab experiment at the depth of 5.0 cm. Because of limits in the the positional reproducibility of the slab inhomogeneity experiment setup (standard deviation = 0.3 mm) and large gradients in the dose falloff, the standard error of the mean dose was as high as 2.5%.

B. Homogeneous water data

The comparisons of the measured and MC-calculated central-axis depth doses in homogeneous water at 100 cm SSD for the 20 and 9 MeV electron beams are shown in Fig. 5. The 20 MeV comparison showed excellent agreement, with the greatest differences at the 90% and 10% depths. At these depths the MC calculations slightly underestimated the measured dose by approximately 1%. The 9 MeV comparison showed excellent agreement ($<1\%$) at depths greater than 0.4 cm.

The isodose comparisons of the measured and MC-calculated dose distributions for the 20 MeV electron beam

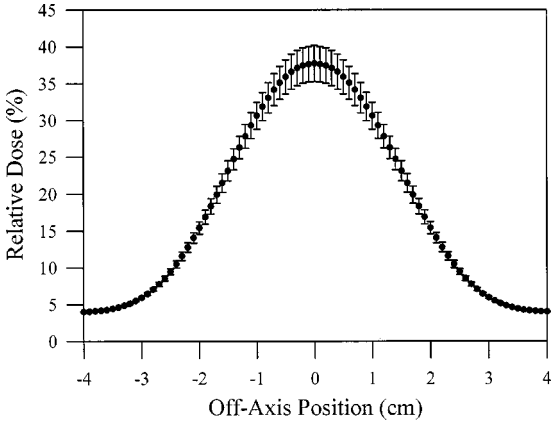

FIG. 4. Dose profile at the 5.0 cm depth for the 9 MeV air-slab experiment. Error bars indicate one standard deviation of the mean measured dose at each point.

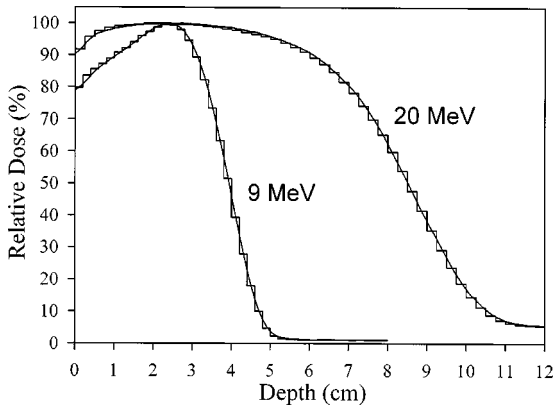

FIG. 5. Comparison of central-axis depth dose for the 9 and the 20 MeV electron beam incident on the homogeneous water phantom at 100 cm SSD. The measured depth doses are shown with the curved lines and MC-calculated depth doses are shown with the stepped line.

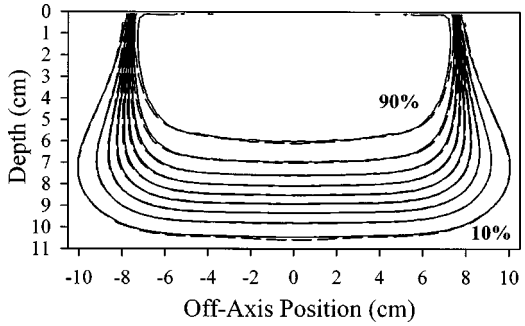

FIG. 6. 20 MeV, 100 cm SSD, homogeneous water experiment. Isodose comparison of measured dose (dashed line) and MC-calculated dose (solid line).

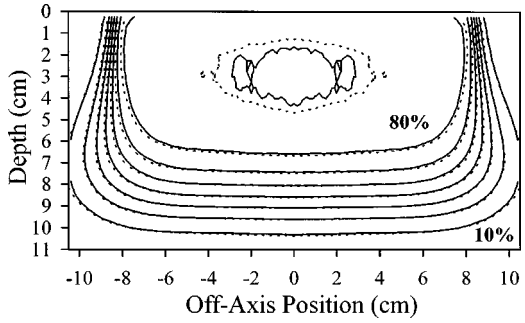

FIG. 7. 20 MeV, 110 cm SSD, homogeneous water experiment. Isodose comparison of measured dose (dotted line) and MC-calculated dose (solid line).

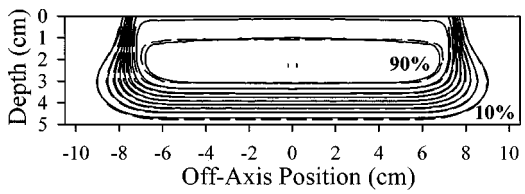

FIG. 8. 9 MeV, 100 cm SSD, homogeneous water experiment. Isodose comparison of measured dose (dashed line) and MC-calculated dose (solid line).

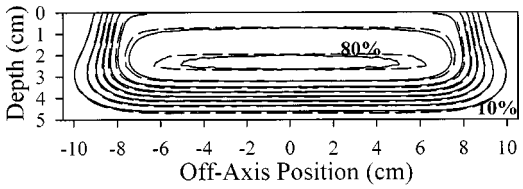

FIG. 9. 9 MeV, 110 cm SSD, homogeneous water experiment. Isodose comparison of measured dose (dashed line) and MC-calculated dose (solid line).

at 100 and 110 cm SSD in water are shown in Figs. 6 and 7, respectively. Within the central region of the distributions, the agreement was within 2%. Regions with dose differences greater than 2% were seen in the penumbra, with most of the data being within the 1 mm DTA criteria; points that were not within the 1 mm DTA criteria had dose differences no greater than 2.5%. The dose differences in the penumbra can be attributed to high-dose gradients and to a previously noted deficiency in the ability of our BEAM accelerator model to predict dose profiles just inside the field edges.[14] The deficiency in the BEAM accelerator model is also apparent in the results of the extended SSD comparison. The isodose comparisons between the measured and MC-calculated dose distributions for the 9 MeV electron beam at 100 and 110 cm SSD in water are shown in Figs. 8 and 9, respectively. The comparisons of the 9 MeV, 100 cm SSD data showed a 2% or better agreement in the central region of the distribution (± 5 cm lateral to the central axis). The comparisons of the 9 MeV, 110 cm SSD data did not show a 2% or better agreement in the central region of the distribution; however, most of the data were within the 1 mm DTA criteria. The maximum dose difference in the 9 MeV, 110 cm SSD comparison that was not within the 1 mm DTA criteria was 2.5%.

C. Internal inhomogeneity data

In experiments involving the Styrofoam air pocket, the 20 MeV measured data showed very good agreement with MC-calculated dose. Figure 10 shows the isodose comparison for the 20 MeV horizontal air-slab experiment, and Fig. 11 shows the isodose comparison for the 20 MeV vertical air-slab experiment. Both comparisons showed better than 2% agreement within the central region.

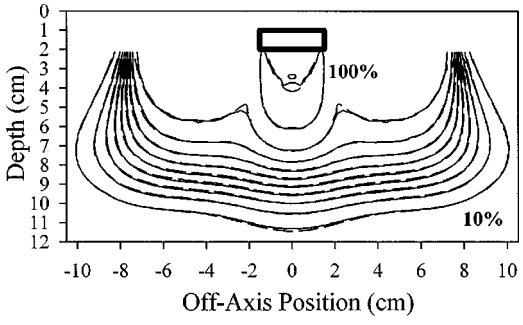

FIG. 10. 20 MeV, horizontal air slab experiment. Isodose comparison of measured dose (dashed) and MC-calculated dose (solid). The thick solid line shows the contour of the air slab.

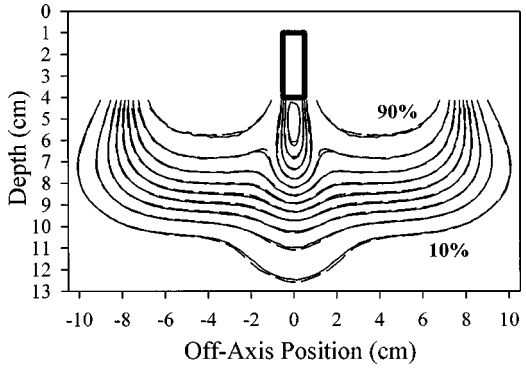

FIG. 11. 20 MeV, vertical air-slab experiment. Isodose comparison of measured dose (dashed line) and MC-calculated dose (solid line). The thick solid line shows the contour of the air slab.

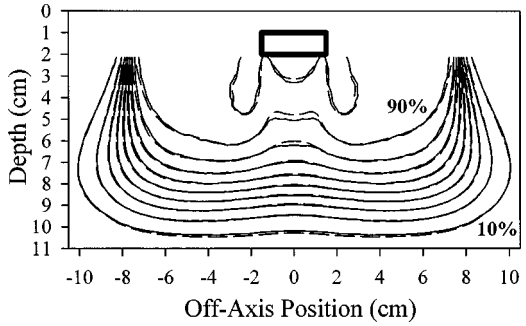

FIG. 12. 20 MeV, horizontal bone-slab experiment. Isodose comparison of measured dose (dashed line) and MC-calculated dose (solid line). The thick solid line shows the contour of the bone slab.

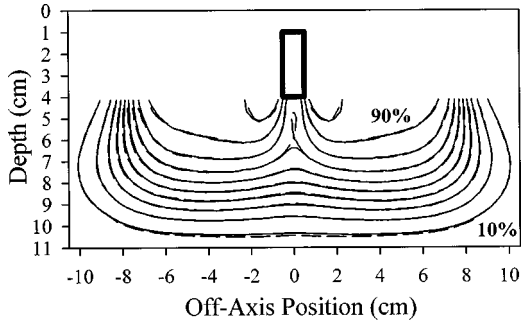

FIG. 13. 20 MeV, vertical bone-slab experiment. Isodose comparison of measured dose (dashed line) and MC-calculated dose (solid line). The thick solid line shows the contour of the bone slab.

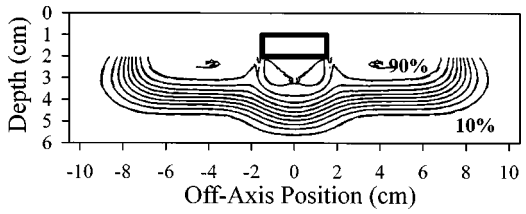

FIG. 14. 9 MeV, horizontal air-slab experiment. Isodose comparison of measured dose (dashed line) and MC-calculated dose (solid line). The thick solid line shows the contour of the air slab.

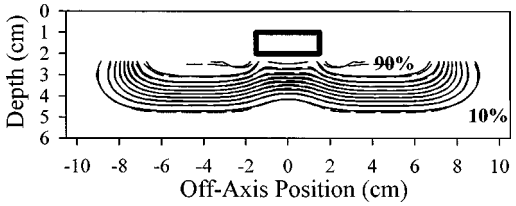

FIG. 15. 9 MeV, horizontal bone-slab experiment Isodose comparison of measured dose (dashed line) and MC-calculated dose (solid line). The thick solid line shows the contour of the bone slab.

In experiments involving the bone slab the 20 MeV measured data showed good agreement with MC data. Figure 12 shows the isodose comparison for the 20 MeV horizontal bone-slab experiment, and Fig. 13 shows the isodose comparison for the 20 MeV vertical bone-slab experiment. Both comparisons showed better than 2% agreement within the central region, except near the central axis in the horizontal bone-slab experiment, where the dose difference reached 2.1%. In the central region of both experiments, the measured dose was slightly lower than the MC-calculated minimum dose value in the shadow of the bone slab.

Agreement with the MC-calculated data was not as good for the 9 MeV internal inhomogeneity data as for the 20 MeV data. Figure 14 shows the isodose comparison for the 9 MeV horizontal air-slab experiment and Fig. 15 shows the isodose comparison for the 9 MeV horizontal bone-slab experiment. Both comparisons showed differences greater than 2% in the dose falloff region in the shadow of the inhomogeneities. In the shadow of the inhomogeneity, the comparisons showed the dose in the falloff region to be less for the measured data than for the MC-calculated data. Although the dose differences were slightly greater than 2% in the shadow of the inhomogeneity, the DTA was within 0.3 mm. Nonetheless, the small dose differences in the shadow of the inhomogeneity could be attributable to multiple possibilities, e.g., insufficient MC modeling, inaccurate value of the physical properties of the slab materials, dependence of the detector sensitivity on the detector position, etc.

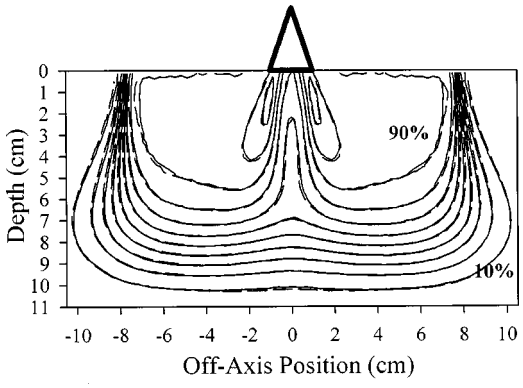

FIG. 16. 20 MeV, nose-shaped-surface experiment. Isodose comparison of measured dose (dashed line) and MC-calculated dose (solid line). The thick solid line shows the contour of the irregular surface.

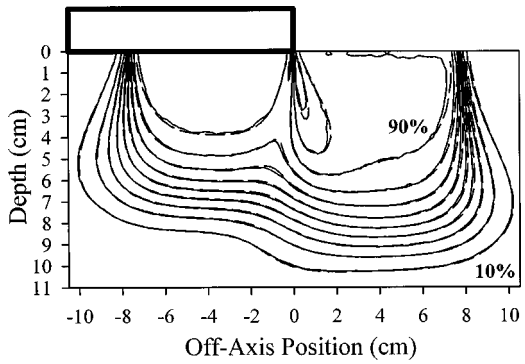

FIG. 17. 20 MeV, 2 cm stepped-surface experiment. Isodose comparison of measured dose (dashed line) and MC-calculated dose (solid line). The thick solid line shows the contour of the irregular surface.

D. Irregular surface data

The isodose comparisons between the measured and MC-calculated dose distributions for the 20 MeV nose-shaped-surface and stepped-surface experiments are shown in Figs. 16 and 17, respectively. The agreement in the central region was better than 2% except in the hot spots near the edges of the nose (1.5 cm lateral to the central axis). The maximum dose difference in the extreme dose values of the nose surface was 2.5%.

The isodose comparisons between the measured and MC-calculated dose distributions for the 9-MeV nose-shaped-surface and stepped-surface experiments are shown in Figs. 18 and 19, respectively. The agreement in the central region is better than 2% except in the hot spots near the edges of the nose (1.5 cm lateral to the central axis) and underneath the Styrofoam block near the field edge following the 90% isodose line. The maximum dose difference in the peak-dose values of the nose surface was 2.3%.

IV. CONCLUSIONS

The beam data measured in the present work showed high levels of precision and accuracy with no evidence of systematic error and is believed suitable for verification of electron dose algorithms. The measured data showed a precision of 0.5% or better.

In general, the measured data matched the MC-generated data to within 2% relative to the normalization dose. A few notable instances where the dose differences were greater

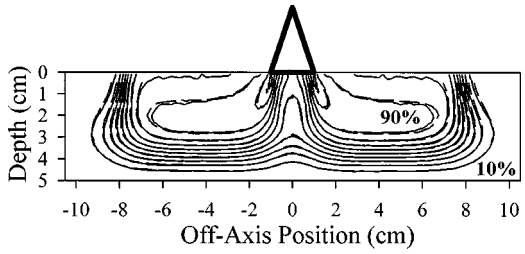

FIG. 18. 9 MeV, nose-shaped-surface experiment. Isodose comparison of measured dose (dashed line) and MC-calculated dose (solid line). The thick solid line shows the contour of the irregular surface.

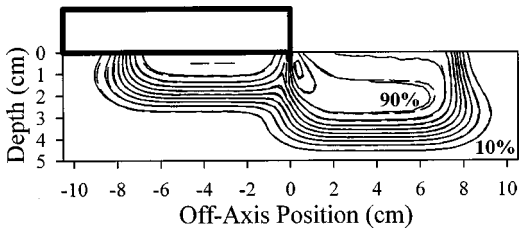

FIG. 19. 9 MeV, 2 cm stepped-surface experiment. Isodose comparison of measured dose (dashed line) and MC-calculated dose (solid line). The thick solid line shows the contour of the irregular surface.

than 2% occurred in the dose falloff region in the shadow of internal inhomogeneities in the 9 MeV data, and the maximum dose peaks of the irregular-surface experiments. Differences slightly greater than 2% also occurred in the penumbra due perhaps to inadequate modeling of the dual foil scattering system,[12] and we believe this to have negligible impact on MC dose accuracy in the central region of the heterogeneity experiments. Most of these points were located in high-dose gradients and were within a DTA of 1 mm. Of the few points at which both criteria were not met, the maximum dose difference was 2.5%. Nonetheless, the agreement between the measured dose and the MC-calculated dose gives a high degree of confidence that both data sets are accurate within 2%. The quality of this data set is superior to that of ECWG data and should allow for better evaluation of the accuracy of an electron beam dose algorithm.[19] We expect that these data will be made available electronically from the Department of Radiation Physics at The University of Texas M. D. Anderson Cancer Center.

Also, the benchmarking of the BEAM/DOSXYZ MC code indicates it to be accurate to within 2% of the measured data, which should allow it to be used to produce dose distributions in actual patients. Such data are the subject of future work to determine the accuracy of the pencil-beam redefinition algorithm for patient treatment planning.

ACKNOWLEDGMENTS

This work was supported in part by the P. H. and Fay Etta Robinson Distinguished Professorship in Cancer Research and by a fellowship from the American Legion Auxiliary. Special thanks goes to Michael Bieda for his excellent help in using BEAM to model the Varian Clinac 2100C and to John Griffin and Nick Zachralopolous for machining the inhomogeneities and other apparatus needed for the phantom geometry configurations.

[1] A. S. Shiu, S. Tung, K. R. Hogstrom, J. W. Wong, R. L. Gerber, W. B. Harms, J. A. Purdy, R. K. Ten Haken, D. L. McShan, and B. A. Fraass, ''Verification data for electron beam dose algorithms,'' Med. Phys. **19**, 623–636 (1992).

[2] D. L. McShan, B. A. Fraass, and R. K. Ten Haken, ''Dosimetric verification of a 3-D electron pencil beam dose calculation,'' Med. Phys. **21**, 13–23 (1994).

[3] A. Cheng, W. B. Harms, R. L. Gerber, J. W. Wong, and J. A. Purdy, ''Systematic verification of a three-dimensional electron beam dose calculation algorithm,'' Med. Phys. **23**, 685–693 (1996).

[4] B. Fraass, K. Doppke, M. Hunt, G. Kutcher, G. Starkschall, R. Stern, and J. Van Dyke, ''American Association of Physicists in Medicine Radiation

Therapy Committee Task Group 53: Quality assurance for clinical radiotherapy treatment planning,'' Med. Phys. **25**, 1773–1829 (1998).
[5] M. Fippel, I. Kawrakow, and K. Friedrich, ''Electron beam dose calculations with the VMC algorithm and the verification data of the NCI working group,'' Phys. Med. Biol. **42**, 501–520 (1997).
[6] A. Samuelsson, S. Hyödynmaa, and K.-A. Johansson, ''Dose accuracy check of the 3D electron beam algorithm in a treatment planning system,'' Phys. Med. Biol. **43**, 1529–1544 (1998).
[7] R. Muller-Runkel and S.-H. Cho, ''Evaluation of a commercial three-dimensional electron pencil beam algorithm,'' Med. Phys. **24**, 91–101 (1997).
[8] G. X. Ding, J. E. Cygler, G. G. Zhang, and M. K. Yu, ''Evaluation of a commercial three-dimensional electron beam treatment planning system,'' Med. Phys. **26**, 2571–2580 (1999).
[9] E. W. Korevaar, A. Akhiat, B. J. M. Heijmen, and H. Huizenga, ''Accuracy of the phase space evolution dose calculation model for clinical 25 MeV electron beams,'' Phys. Med. Biol. **45**, 2931–2946 (2000).
[10] R. A. Boyd, ''The effect of using an initial polyenergetic spectrum with the electron pencil-beam redefinition algorithm,'' M.S. thesis, The University of Texas Health Science Center-Houston, Graduate School of Biomedical Sciences, 1997.
[11] D. W. O. Rogers, B. A. Faddegon, G. X. Ding, C. M. Ma, J. We, and T. R. Mackie, ''BEAM: A Monte Carlo code to simulate radiotherapy treatment units,'' Med. Phys. **22**, 503–524 (1995).
[12] K. R. Shortt, C. K. Ross, A. F. Bielajew, and D. W. O. Rogers, ''Electron beam dose distributions near standard inhomogeneities,'' Phys. Med. Biol. **31**, 235–249 (1986).
[13] A. Kapur, C.-M. Ma, E. C. Mok, D. O. Findley, and A. L. Boyer, ''Monte Carlo calculations of electron beam output factors for a medical linear accelerator,'' Phys. Med. Biol. **43**, 3479–3494 (1998).
[14] M. R. Bieda, ''A Monte Carlo method for commissioning electron beams,'' M.S. thesis. The University of Texas Health Science Center-Houston, Graduate School of Biomedical Sciences, 1999.
[15] F. M. Khan, K. P. Doppke, K. R. Hogstrom, G. J. Kutcher, R. Nath, S. C. Prasad, J. A. Purdy, M. Rozenfeld, and B. L. Werner, ''Clinical electron-beam dosimetry: Report of AAPM Radiation Therapy Committee Task Group No. 25,'' Med. Phys. **18**, 73–109 (1991).
[16] C. Constantinou, ''Tissue substitutes for particulate radiations and their use in radiation dosimetry and radiotherapy,'' Ph.D. thesis, The University of London, 1978.
[17] D. A. Jaffray, J. J. Battista, A. Fenster, and P. Munro, ''X-ray sources of medical linear accelerators: Focal and extra-focal radiation,'' Med. Phys. **20**, 1417–1427 (1993).
[18] F. García-Vincente, J. M. Delgado, and C. Peraza, ''Experimental determination of the convolution kernel for the study of the spatial response of a detector,'' Med. Phys. **25**, 202–207 (1998).
[19] R. A. Boyd, G. Starkschall, and K. R. Hogstrom, ''Pencil-beam redefinition algorithm dose calculations in the presence of heterogeneities,'' Med. Phys. (submitted).